catalysts

MDPI

Article

Alkaline Modification of a Metal–Enzyme–Surfactant Nanocomposite to Enhance the Production of L-α-glycerylphosphorylcholine

Hui Li [1,2], Xun Cao [3], Yuanyuan Lu [1,2], Yan Ni [1,2], Xin Wang [1,2], Qiuhao Lu [1,2], Ganlu Li [1,2], Kequan Chen [1,2,*], Pingkai Ouyang [1,2] and Weimin Tan [4]

1 College of Biotechnology and Pharmaceutical Engineering, Nanjing Tech University, Nanjing 211816, China; lihui11@njtech.edu.cn (H.L.); lyy940812@163.com (Y.L.); niyan92@163.com (Y.N.); xinwang1988@njtech.edu.cn (X.W.); luqiuhao@njtech.edu.cn (Q.L.); tkscb@163.com (G.L.); ouyangpk@njtech.edu.cn (P.O.)
2 State Key Laboratory of Materials-Oriented Chemical Engineering, Nanjing Tech University, Nanjing 211816, China
3 Department of Chemical Engineering, Tsinghua University, Beijing 100084, China; cx0118@hotmail.com
4 National Engineering Research Center for Coatings, CNOOC Changzhou Paint and Coatings Industry Research Institute Co., Ltd, Changzhou 213016, China; atan0910@163.com
* Correspondence: kqchen@njtech.edu.cn

Received: 21 January 2019; Accepted: 27 February 2019; Published: 4 March 2019

Abstract: Microenvironment modification within nanoconfinement can maximize the catalytic activity of enzymes. Phospholipase A_1 (PLA_1) has been used as the biocatalyst to produce high value L-α-glycerylphosphorylcholine (L-α-GPC) through hydrolysis of phosphatidylcholine (PC). We successfully developed a simple co-precipitation method to encapsulate PLA_1 in a metal–surfactant nanocomposite (MSNC), then modified it using alkalescent 2-Methylimidazole (2-Melm) to promote catalytic efficiency in biphasic systems. The generated 2-Melm@PLA_1/MSNC showed higher catalytic activity than PLA_1/MSNC and free PLA_1. Scanning electron microscopy and transmission electron microscopy showed a typical spherical structure of 2-Melm@PLA_1/MSNC at about 50 nm, which was smaller than that of 2-Melm@MSNC. Energy disperse spectroscopy, N_2 adsorption isotherms, Fourier transform infrared spectrum, and high-resolution X-ray photoelectron spectroscopy proved that 2-Melm successfully modified PLA_1/MSNC. The generated 2-Melm@PLA_1/MSNC showed a high catalytic rate per unit enzyme mass of 1.58 μmol mg^{-1} min^{-1} for the formation of L-α-GPC. The 2-Melm@PLA_1/MSNC also showed high thermal stability, pH stability, and reusability in a water–hexane biphasic system. The integration of alkaline and amphiphilic properties of a nanocomposite encapsulating PLA_1 resulted in highly efficient sequenced reactions of acyl migration and enzymatic hydrolysis at the interface of a biphasic system, which cannot be achieved by free enzyme.

Keywords: metal–surfactant nanocomposite; phospholipase A_1; microenvironment modification

1. Introduction

L-α-glycerylphosphorylcholine (L-α-GPC) is an important derivative of phosphatidylcholine (PC) and a promising candidate to treat Alzheimer's disease [1,2]. Enzymatic preparation of L-α-GPC has received more and more attention, especially phospholipase A_1, due to few side effects and easy recovery of products [3–5]. However, the slow 30 h reaction time for the preparation of L-α-GPC via phospholipase A_1(PLA_1)-catalyzed hydrolysis of PC in n-hexane–water biphasic mediais not suitable for industrial applications [4]. The low solubility of PC in water and the slow migration rate

of the acyl group from the *sn*-2 position to the *sn*-1 position result in low productivity of L-α-GPC, limiting the application of PLA_1 in industry [6]. A previous study indicated that an alkaline pH environment can benefit both the acyl migration and hydrolysis process [7]. Therefore, it would be a promising route to increase the productivity of L-α-GPC if biphasic enzymatic catalysis can be achieved with PC solubilized in the organic phase and the enzyme connected with a neighboring alkaline microenvironment.

Enzyme immobilization in biocatalysts shows great advantages including lower risk of product contamination with enzyme residues and enzymes being easy to recycle [8–10]. Further, enzyme immobilization on nanomaterials has demonstrated that many unique and advantageous physicochemical properties of nanostructures can increase catalytic performance and offer new functionality of enzyme catalysts, in addition to enhancing stability and reusability [11–13]. Inorganic crystal nanomaterials such as metal-organic frameworks (MOFs), with advantages of high specific surface area, tunable pores, and diverse functionalities, have shown great potential in enzyme immobilization. Some examples are: Zeolitic imidazolate framework-8 (ZIF-8) [14,15], Ni-based metal-organic framework nanorods (Fe_3O_4/Ni-BTC) [16], Fe-MIL-88 [17],UiO-66 [18], ZIF-67 [19], MIL-101(Cr) [20],magnetic-MOF [21], Co-TCPP(Fe) nanosheets (Co-FeMOF) [22], PCN-333(Fe), ZIF-90, ZIF-10, NU-1000, and HKUST-1 [23–25]. The confined encapsulation of enzymes in rigid MOFs can protect the enzyme from denaturation and degradation in extreme conditions [26]. Therefore, it is anticipated that immobilizing PLA_1 on a specific nanostructure has the potential to address the above-mentioned challenge of industrial production of L-α-GPC.

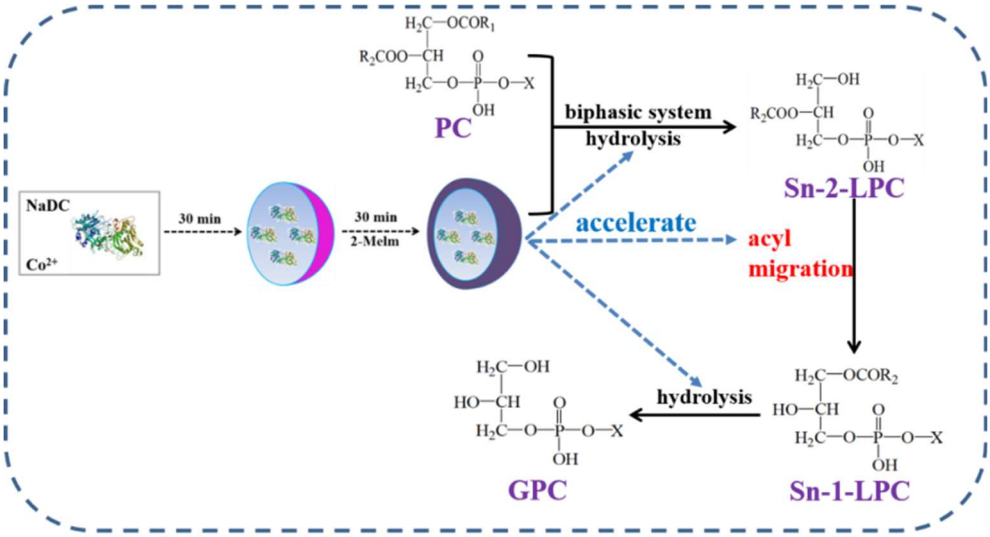

Scheme 1. Schematic synthesis and catalytic performance of a 2-Methylimidazolephospholipase A_1metal–surfactant nanocomposite(2-Melm@PLA_1/MSNC).

The microenvironment in nanostructures plays an important role in enzymatic activity [27–29]. The microenvironmental modification of nanocarriers can enhance the enzymatic catalytic activity and catalytic performance characteristics, which has received more and more attention [30–33]. ε-Poly-L-lysine (EPL)-modified mesoporous titanium dioxide (M-TiO_2) with negative charges for immobilized enzymes displayed strong storage stability, thermal stability, and good reusability [28]. The enzymeZIF-8 treated with salt ions showed enhanced activity, storage stability, and the ability to resist against trypsin [29]. We have successfully prepared a novel enzyme–metal–surfactant nanocomposite, which demonstrated strong catalytic activity, storage stability, thermal stability, and good reusability in highly polar solvents and deep eutectic solvents [34–36]. Under these considerations, we proposed using metal ions and organic surfactants to construct a metal–surfactant nanocomposite capable of simultaneously encapsulating enzymes, followed by subsequent coordinating modification

of the nanocomposite with alkalescent 2-Methylimidazole (2-Melm). Microenvironment modification within nanoconfinement can maximize the catalytic activity of enzymes (Scheme 1). We hypothesize that the nanocomposite made of surfactants has an amphiphilic nature and can localize in the interface to catalyze a biphasic reaction. At the same time, the presence of 2-Melm in the nanocomposite would provide an alkalescent microenvironment for facilitating the tandem acyl migration and hydrolysis process.

2. Results and Discussion

2.1. Effect of 2-Melm on PLA_1/MSNC Activity

The catalytic performance of 2-Methylimidazolephospholipase A_1metal–surfactant nanocomposite (2-Melm@PLA_1/MSNC) with 50 nm sample size in 5 mL biphasic reaction system containing 50% (v/v) organic solvents was investigated in the production of L-α-GPC. First, the influence of organic solvents (including isooctane, heptane, hexane, 1-hexanol, and butanol) in the biphasic enzymatic catalysis of 2-Melm@PLA_1/MSNC and free $PLA_1$was studied (Table 1). No L-α-GPC was produced in any biphasic systems catalyzed by free PLA_1. In contrast, the yields of L-α-GPC catalyzed by 2-Melm@PLA_1/MSNC in the water–isooctane, water–heptane, water–hexane, and water–1-hexanol biphasic systems reached 341.02 ± 11.21, 559.84 ± 16.82, 919.96 ± 35.68, and 239.73 ± 15.79 μmolL^{-1}, respectively, within 30 min. These results indicated that a water–hexane biphasic system was the best reaction medium, which is consistent with previously reported results [4].

Table 1. Effects of organic solvents on the L-α-glycerylphosphorylcholine (L-α-GPC) yield catalyzed by 2-Melm@PLA_1/MSNC and freePLA_1.

Solvent	Log P	Yield (μmolL^{-1})	
		Free PLA_1	2-Melm@PLA_1/MSNC
Isooctane	4.5	0	341.02 ± 11.21
Heptane	4.0	0	559.84 ± 16.82
Hexane	3.5	0	919.96 ± 35.68
1-Hexanol	1.8	0	239.73 ± 15.79
Butanol	0.8	0	0

Footnote: The values were taken from the triplicate samples.

The yield of L-α-GPC catalyzed by PLA_1/MSNC without modification of 2-Melm in the water–hexane system was 203.86 ± 7.90 μmolL^{-1} (Figure 1a). A previous study showed that MSNC is a new kind of surfactant containing two types of metal ions [34], which could both reduce the interfacial tension of the water–hexane system and increase the solubility of PC. Therefore, after encapsulation in MSNC, the PLA_1/MSNC nanocomposite maintained the surfactant-like property and was localized at the water–hexane interface, greatly enhancing the accessibility of substrates solubilized in the organic phase towards the active site of the enzyme [34]. This is one of the reasons that, after encapsulation, PLA_1/MSNC increased apparent activity in the production of L-α-GPC compared to free PLA_1. As another control experiment, the addition of 2-Melm in the reaction system catalyzed by PLA_1/MSNC also contributed to enhanced catalytic activity of PLA_1 (Figure 1a). During the hydrolysis, migration of the acyl group from the *sn*-2 position to the *sn*-1 position occurred due to the lower thermodynamic stability of *sn*-1-lysophosphatidylcholine(*sn*-1-LPC) compared to *sn*-2-LPC (Scheme 1) [4]. In addition, 2-Melm@PLA_1/MSNC had higher catalytic activity than the mixture of PLA_1/MSNC and 2-Melm (Figure 1a), possibly because the modification of 2-Melm in the nanocomposite resulted in a proximity effect between enzymatic hydrolysis and acyl group migration, which further improved the catalytic performance of the system [35,37,38].

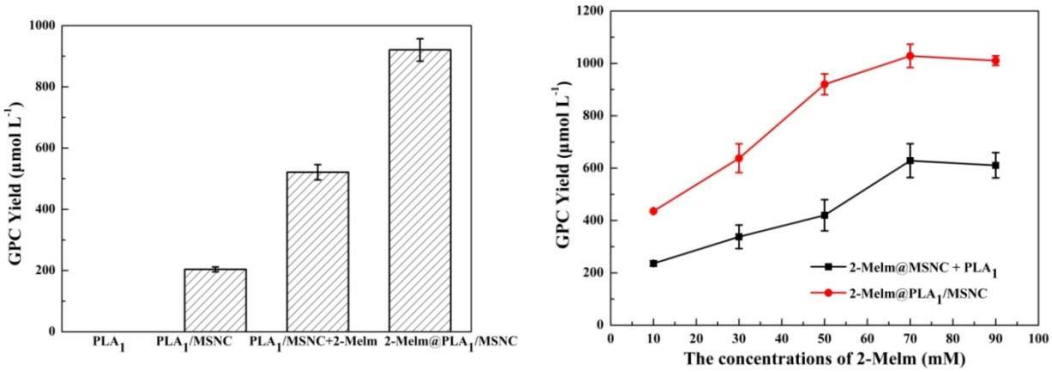

(**a**) (**b**)

Figure 1. (**a**) Comparison of the yields of L-α-GPC catalyzed by different enzyme samples; (**b**) the effect of 2-Melm concentration in self-assembly of the nanocomposite on the yield of L-α-GPC catalyzed by 2-Melm@PLA_1/MSNC and the mixture of 2-Melm@MSNC and PLA_1.

The effect of the concentration of 2-Melm in self-assembly of the nanocomposite on the yield of GPC catalyzed by 2-Melm@PLA_1/MSNC and the mixture of 2-Melm@MSNC and PLA_1 is displayed in Figure 1b. The optimal concentration of 2-Melm in self-assembly of the nanocomposite was 70 mM. The optimal concentration of 2-Melm formed the optimum alkaline catalytic microenvironment in the nanocomposite. The presence of alkaline groups can catalyze acyl migration [7]. In addition, 2-Melm@PLA_1/MSNC had higher catalytic activity than the mixture of 2-Melm@MSNC and PLA_1at the same concentration of 2-Melm. Thus, the addition of 2-Melm in the reaction system catalyzed the migration of the acyl group and increased productivity. After modification with 2-Melm, 2-Melm@PLA_1/MSNC had the two above-mentioned benefits: interfacial catalysis and facilitated acyl group migration. Microenvironmental modification aimed at enhancing the catalytic reaction of enzymes in specific reaction media is an important method to improve the activity of immobilized enzymes [30–33]. The modification of 2-Melm maintained the alkaline microenvironment of 2-Melm@PLA_1/MSNC in the nanostructure, which was more suitable for the catalytic conditions of PLA_1. The coupling of microenvironment and catalytic conditions can maximize the catalytic activity of the catalyzer [39,40].

2.2. Characterization of 2-Melm@PLA_1/MSNC

Scanning electron microscopy (SEM) images, transmission electron microscopy (TEM) images, and energy disperse spectroscopy (EDS) data revealed differences in morphology and composition between the nanocomposite with and without enzyme encapsulation.SEM and TEM images showed a typical spherical structure of 2-Melm@PLA_1/MSNC at about 50 nm. The SEM images showed that the particle size of 2-Melm@PLA_1/MSNC was smaller than that of 2-Melm@MSNC (Figure 2a,b), possibly because the coordination interaction between protein and metal ions resulted in the formation of a more compact structure in the self-assembly process. In TEM images (Figure 2c,d), the 2-Melm@PLA_1/MSNC displayed more regions with light electron density due to the encapsulation of protein molecules [41]. Moreover, the EDS data also demonstrated that protein molecules (containing P and S elements) were successfully embedded in the nanocomposite (Figure 2e,f).

N_2 adsorption isotherms measured at 77 K identified differences in porous features between nanocomposites with and without enzyme encapsulation (Figure 3a). The data showed that the Brunauer–Emmett–Teller (BET) surface area (81.08 m^2 g^{-1}) and pore volume (0.69 cm^3 g^{-1}) of 2-Melm@PLA_1/MSNC were larger than that of 2-Melm@MSNC (Table 2), demonstrating that incorporating protein and coordination between the enzyme and Co^{2+} affected the porous structure of the nanocomposite [34,35].

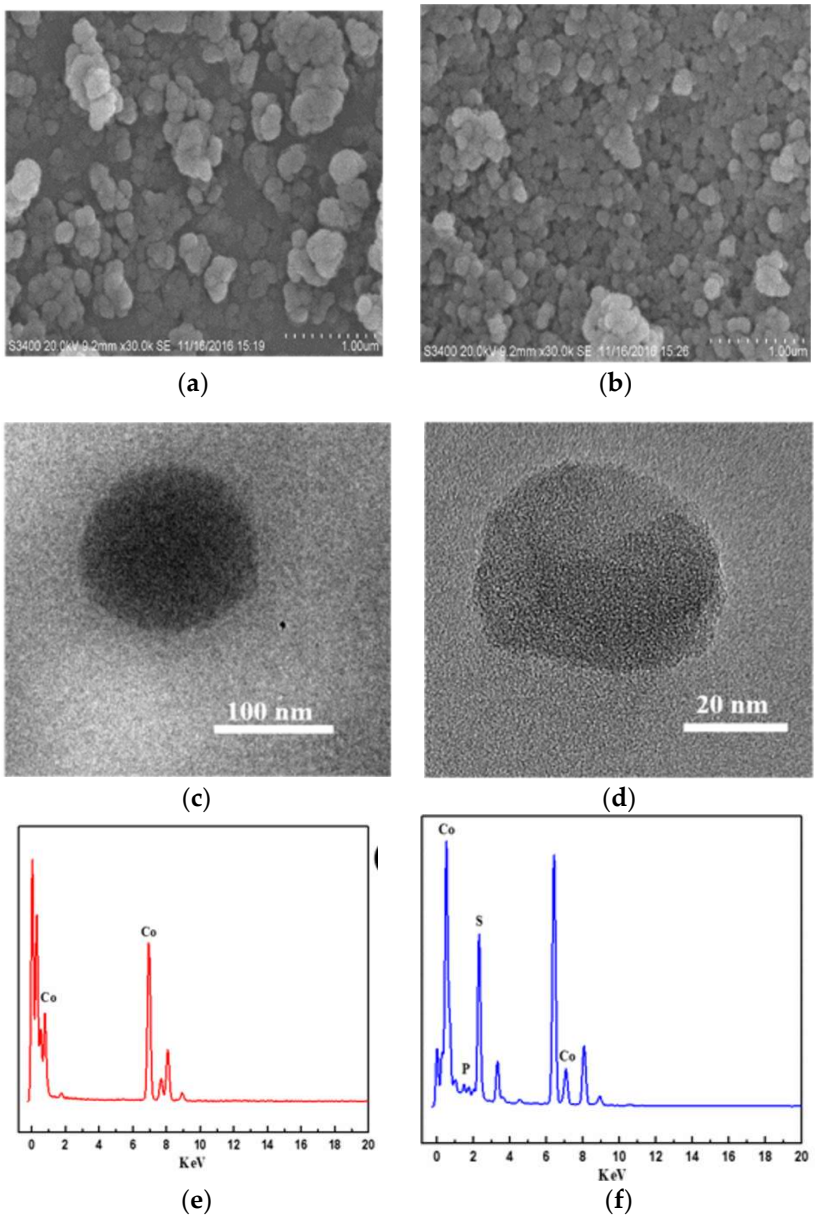

Figure 2. (**a**) SEM image of 2-Melm@MSNC; (**b**) SEM image of 2-Melm@PLA_1/MSNC; (**c**) TEM image of 2-Melm@MSNC; (**d**) TEM image of 2-Melm@PLA_1/MSNC; (**e**) EDS of 2-Melm@MSNC; (**f**) EDS of 2-Melm@ PLA_1/MSNC.

Table 2. Brunauer–Emmett–Teller (BET) surface area, average pore volume, and pore width of 2-Melm@MSNC and 2-Melm@PLA_1/MSNC.

Sample	BET Surface Area(m^2g^{-1})	Average Pore Volume(cm^3g^{-1})	Average Pore Width(nm)
2-Melm@MSNC	48.76	0.22	25.23
2-Melm@PLA_1/MSNC	81.08	0.69	28.69

As observed in the Fourier transform infrared (FTIR) spectrum (Figure 3b), the presence of C=N stretching vibration at 1560 cm^{-1} and out-of-plane bending mode at 755 cm^{-1} (from 2-Melm) demonstrated that MSNC or PLA_1/MSNC was successfully modified by2-Melm [42]. Compared with 2-Melm@MSNC, the FTIR spectra of 2-Melm@PLA_1/MSNC displayed an enhanced adsorption peak at 1654 cm^{-1} that represented the C=O vibration of the amide I band, and a secondary amine of amide

N–H stretch based on splitting of the peak between 3250–3500 cm^{-1} in PLA_1 [43], indicating that PLA_1 was successfully immobilized in the nanocomposite. The 2-Melm@PLA_1/MSNC also showed an enhanced peak at 2800–3000 cm^{-1} of the C–H vibration.

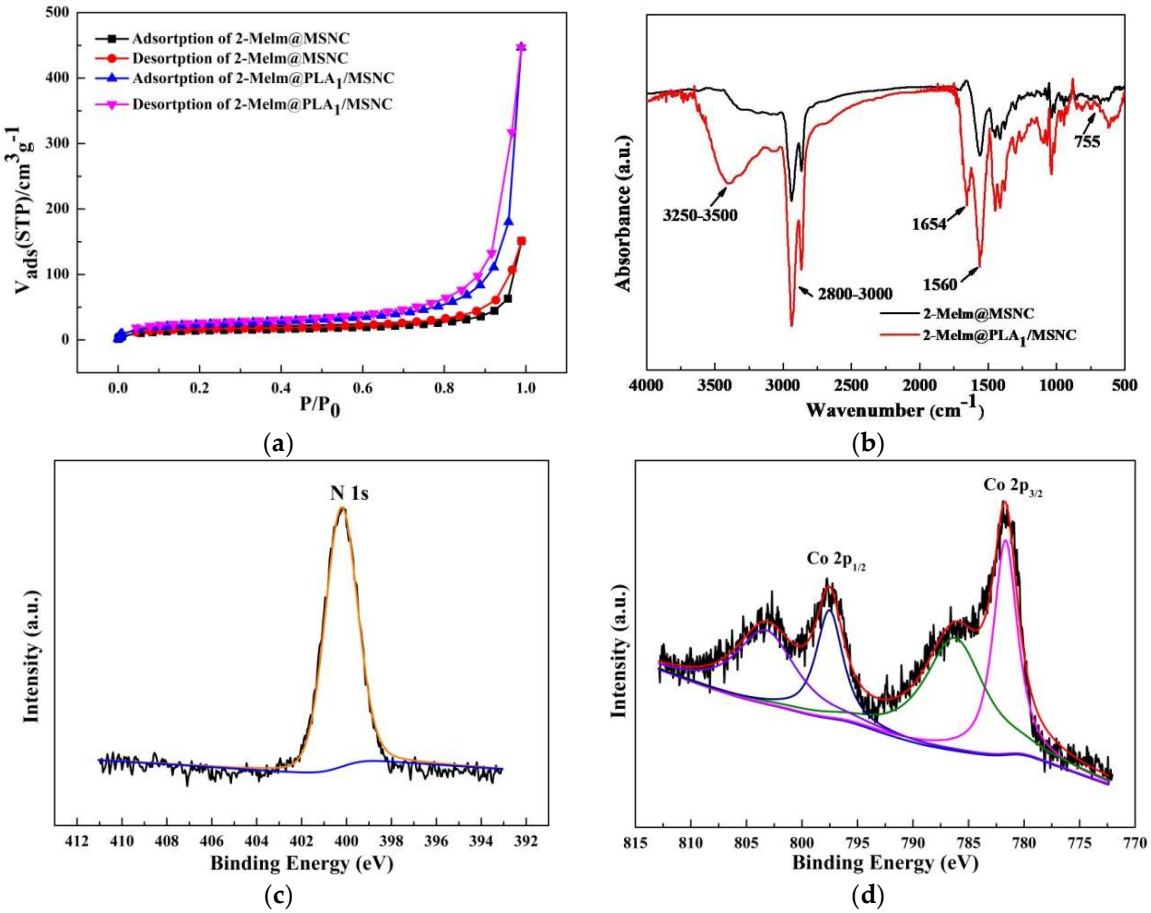

Figure 3. (**a**) N_2 adsorption isotherm of 2-Melm@MSNC and 2-Melm@PLA_1/MSNC; (**b**) FTIR spectra of 2-Melm@MSNC and 2-Melm@PLA_1/MSNC; (**c**) high-resolution XPS spectra of N 1s of 2-Melm@PLA_1/MSNC; (**d**) high-resolution XPS spectra of Co 2p of 2-Melm@PLA_1/MSNC.

High-resolution X-ray photoelectron spectroscopy (XPS) revealed composition details of the nanocomposite. The chemical states of Co and N in the surface of the nanocomposite were measured. The N 1s spectrum could be deconvoluted into one peak centered at the binding energy of 400.2 eV, which was assigned to pyrrolic N from 2-Melm, while the predominance of pyrrolic N resulted from coordination with cobalt ions (Figure 3c) [42]. The XPS spectrum of Co $2p_{3/2}$ was characteristic of Co^{2+} species (Figure 3d). Two major peaks with binding energies of 781.7 eV and 797.5 eV were observed in the XPS peak for Co 2p, corresponding to Co $2p_{3/2}$ and Co $2p_{1/2}$. Two small and indistinct peaks at 786.6 and 802.78 eV were typical Co^{2+} shakeup satellite peaks of Co^{2+} and the Co–Nx peak existed at around 788.2 eV [44–46]. The results suggested that 2-Melm was successfully combined with Co^{2+} via metal-coordination interactions on the surface of the nanocomposite.

2.3. Enzymatic Activities of 2-Melm@PLA_1/MSNC

The effects of temperature, stirring rate, and pH on the yield of L-α-GPC catalyzed by 2-Melm@PLA_1/MSNC in a water–hexane biphasic system were investigated in detail. The optimal temperature for 2-Melm@PLA_1/MSNC was 55°C, which was higher than for free PLA_1 according to the literature [4]. The optimal stirring rate was 900 rpm and the optimal pH was 8 (Figure 4a–c). High stirring rate can promote mass transfer in biphasic enzymatic catalysis [47,48].

However, the further increase of stirring rate from 900 to 1000 rpm could result in fracture of the nanocomposite [36,49] and the dissociation of 2-Melm or PLA_1, resulting in a significant reduction of catalytic activity. A weakly alkaline environment (pH 8) can promote the catalytic activity of PLA_1 and result in higher L-α-GPC yield. Compared with published studies, the catalytic rate per unit enzyme mass of the formation of L-α-GPC was 1.58 μmol mg^{-1} min^{-1}, which was faster than the previously reported result (0.89 μmol mg^{-1} min^{-1}) [4].

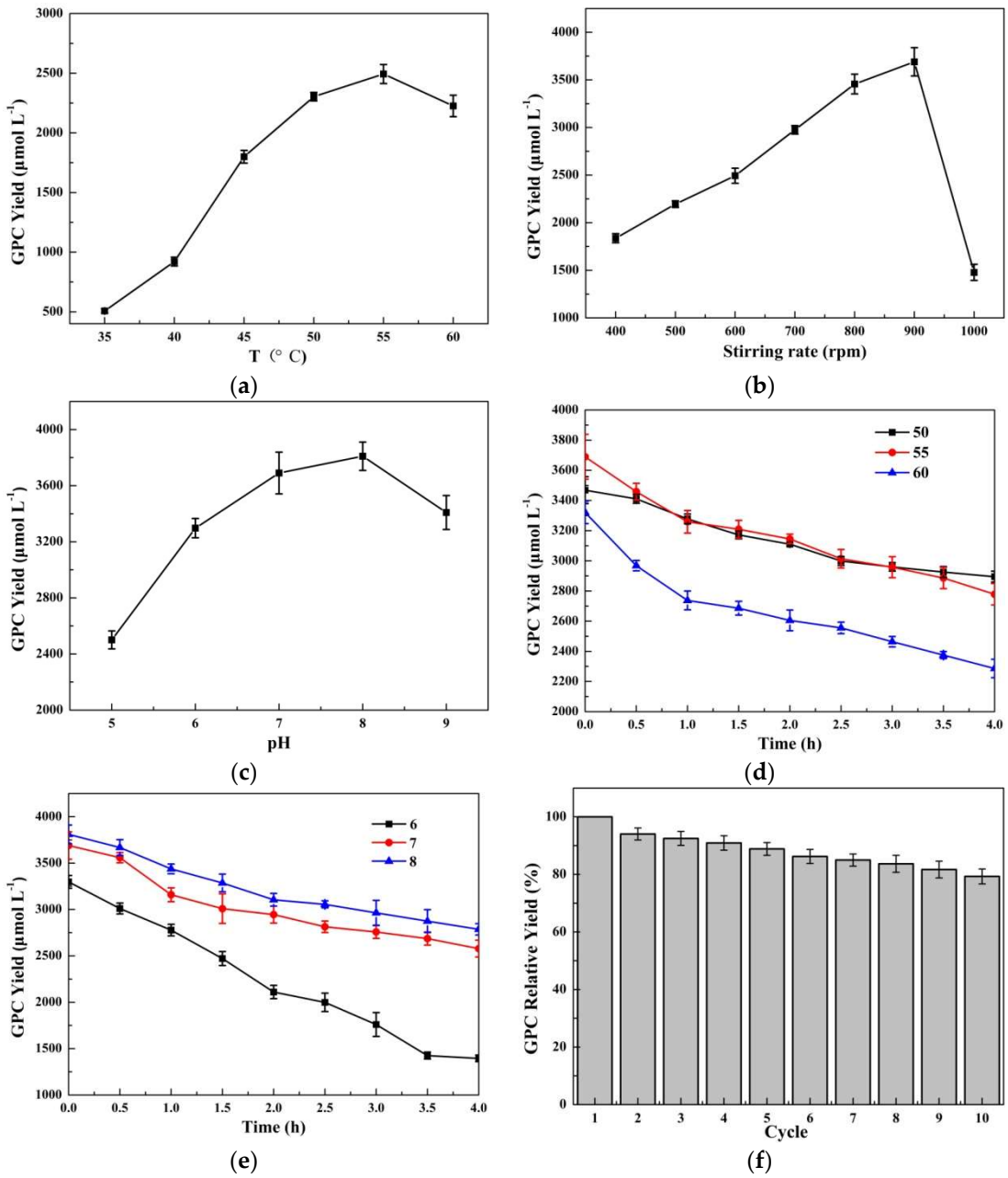

Figure 4. (**a**) The effect of temperature on the yield of L-α-GPC catalyzed by 2-Melm@PLA_1/MSNC; (**b**) the effect of stirring rate on the yield of L-α-GPC catalyzed by 2-Melm@PLA_1/MSNC; (**c**) the effect of pH on the yield of L-α-GPC catalyzed by 2-Melm@PLA_1/MSNC; (**d**) the thermal stability of 2-Melm@PLA_1/MSNC on the yield of L-α-GPC; (**e**) the pH stability of 2-Melm@PLA_1/MSNC on the yield of L-α-GPC; (**f**) the reusability of 2-Melm@PLA_1/MSNC on the yield of L-α-GPC.

The thermal stability and pH stability of 2-Melm@PLA_1/MSNC on the yield of L-α-GPC are shown in Figure 4d,e. Higher catalytic temperature (60°C) for a long time led to lower catalytic activity

of 2-Melm@PLA_1/MSNC, while lower catalytic temperature (50°C) was more conducive to long-term catalysis of 2-Melm@PLA_1/MSNC in the biphasic enzymatic catalysis. In acidic environments (pH 6), acid ions neutralized the alkalinity of 2-Melm, resulting in a decrease in catalytic activity of PLA_1. In neutral (pH 7) and alkaline (pH 8) environments, the alkalinity of 2-Melm increased the activity of PLA_1, resulting in an increase in L-α-GPC yield. Compared with unmodified nanocomposite, modification of 2-Melm in the nanocomposite increased the structural strength, organic solvent tolerance, and alkali resistance. After ten reuses, 2-Melm@PLA_1/MSNC still maintained high catalytic activity and L-α-GPC yield. The reusability of 2-Melm@PLA_1/MSNC showed high stability and structural strength (Figure 4f), indicating high potential for industrial applications [50,51].

3. Materials and Methods

3.1. Materials

Phospholipase A_1 was purchased from Novozymes (Durham, NC, USA). Sodium deoxycholate (NaDC) was obtained from Sinopharm Chemical Reagent Company (Shanghai, China). Cobalt chloride was purchased from Guangdong Chemical Reagent Engineering-technological Research and Development Center (Guangzhou, China). 2-Methylidazole was obtained from Sigma-Aldrich (St. Louis, MO, USA). Food-grade egg-yolk lecithin powder (~70% phosphatidylcholine) was purchased from Meryas limited company (Beijing, China). Other chemicals were of analytical grade.

3.2. PLA_1/MSNC,2-Melm@MSNC, and 2-Melm@PLA_1/MSNCSynthesis

The preparation of 2-Melm@PLA_1/MSNC is shown schematically in Scheme 1. In a typical experiment, 10 mL aqueous solution containing 10 mM sodium deoxycholate (NaDC) and 0.75 $mgmL^{-1}$ (protein concentration) PLA_1 was added to 10 mL water solution containing 20 mM cobalt chloride. After stirring at 300 rpm for 30 min at 25 °C, 10 mL aqueous solution containing different concentrations (10, 30, 50, 70, and 90 mM) 2-Melm was added. After stirring for another 30 min at 25 °C, the mixture was centrifuged at 7000× *g* for 10 min and washed with water twice to obtain the PLA_1/MSNC (without 2-Melm),2-Melm@MSNC (without PLA_1), and 2-Melm@PLA_1/MSNC. The loading amount of PLA_1 in 2-Melm@PLA_1/MSNC and PLA_1/MSNC was determined by the Bradford method to measure the concentration of protein remaining in the supernatant after encapsulation.

3.3. Protein Encapsulation Ratio

The protein contents in the enzyme solutions and encapsulated enzyme preparations were determined according to the Bradford method, using bovine serum albumin as the standard. The assay mixture consisted of 4 mL of Bradford reagent and 1 mL of test solution. The absorbance was read after 3 min at 25 °C standing at 595 nm. The protein encapsulation ratio of the PLA_1/MSNC or 2-Melm@PLA_1/MSNC preparations was calculated indirectly from the difference between the amount of enzyme introduced into the reaction mixture and the amount of enzyme in the filtrate after encapsulation.

3.4. Characterization

The morphologies of the samples were characterized by SEM (S-3400 II; Hitachi, Tokyo, Japan) using an accelerating voltage of 30 kV with fit magnification. For TEM, sample preparation was accomplished by dispersing the composite in ethanol with ultrasound and then placing a well-dispersed droplet on a copper grid. Samples were then dried and analyzed on a JEM-2010 transmission electron microscope (Tokyo, Japan). Analysis of the chemical functional groups of 2-Melm@MSNC and 2-Melm@PLA_1/MSNC were conducted by means of FTIR spectroscopy (Nicolet Is5; Thermo Fisher Scientific). Each sample was ground thoroughly with potassium bromide, and the resulting powder was pressed to form a transparent pellet using a hydraulic press. FTIR spectra were collected in transmission mode between 500 cm^{-1} and 4000 cm^{-1} at a resolution of 2 cm^{-1}.

The binding energies between atoms of 2-Melm@PLA_1/MSNC were measured by high-resolution X-ray photoelectron spectroscopy (ESCALAB 250 Xi).

3.5. PLA_1-Catalyzed Synthesis of L-α-GPC

An enzymatic reaction was performed using 1.5 g egg-yolk lecithin powder and 100 μL free PLA_1 or an equivalent quantity (in terms of protein) of 2-Melm@PLA_1/MSNC (15 mg) or PLA_1/MSNC (7.5 mg) in 2.5 mL phosphate buffer and 2.5 mL organic solvent in a tightly closed 10 mL plastic tube. The tube was incubated in a water bath at 35–60°C, agitated with mechanical stirring at 400–1000 rpm, and pH at 5–9 with 0.1 M phosphate buffer for 30 min.

3.6. High-Performance Liquid Chromatography (HPLC) Analysis

Quantitative analyses of the reactants and products were conducted using a HPLC system from Agilent Technologies (Santa Clara, CA, USA). A reversed-phase column (Zorbax Rx-SIL; 250 mm × 4.6 mm, 5-μm diameter) was used, and the reactants and products were detected by ELSD detector (Agilent 1260). A mixture of methanol/water [90/10 (v/v)] was used as an eluent at 25 °C, with a flow rate of 1 mL min^{-1}.

4. Conclusions

In summary, we successfully synthesized a new type of phospholipase A_1-encapsulated metal–surfactant nanocomposite modified by 2-Melmwith both an alkaline and amphiphilic nature. The nanocomposite2-Melm@PLA_1/MSNC displayed higher catalytic efficiency than PLA_1/MSNC in sequenced reactions of acyl migration and enzymatic hydrolysis at the interface of a biphasic system. Modification of 2-Melm enhanced the catalytic activity of PLA_1 in nanocomposite and resulted in high L-α-GPC yield in a water–hexane biphasic system. Due to the high thermal stability, pH stability, and reusability in a biphasic system, the 2-Melm@PLA_1/MSNC showed high potential for industrial applications. This study gives an example of the potential of using nanomaterials to re-engineer the capability of an enzyme for industrial applications.

Author Contributions: Data curation, Y.L and Y.N.; Formal analysis, Q.L.; Funding acquisition, H.L., X.W., K.C. and P.O.; Investigation, X.C.; Methodology, G.L.; Resources, K.C. and W.T.; Writing—original draft, H.L. and X.C.

Funding: The authors gratefully recognize financial support from the National Key Research and Development Program (2016YFA0204300, 2014AA021703), the National Natural Science Foundation of China (21706126, 21606127, 21576134, and 21390200) and the Jiangsu Synergetic Innovation Center for Advanced Bio-Manufacture (XTE1853).

Conflicts of Interest: The authors declare no conflict of interest.

Abbreviations

L-α-GPC, L-α-glycerylphosphorylcholine; PC, phosphatidylcholine; PLA_1, phospholipase A_1; MOFs, metal-organic frameworks; 2-Melm, 2-Methylimidazole; NaDC, sodium deoxycholate; 2-Melm@PLA_1/MSNC, PLA_1-encapsulated metal-surfactant nanocomposite modified by 2-Melm; PLA_1/MSNC, PLA_1-encapsulated metal-surfactant nanocomposite; 2-Melm@MSNC, metal-surfactant nanocomposite modified by 2-Melm;SEM, scanning electron microscopy; TEM, transmission electron microscopy; EDS, energy disperse spectroscopy; FTIR, Fourier transform infrared spectroscopy; XPS, X-ray photoelectron spectroscopy.

References

1. Lee, S.H.; Choi, B.Y.; Kim, J.H.; Kho, A.R.; Sohn, M.; Song, H.K.; Choi, H.C.; Suh, S.W. Late treatment with choline alfoscerate (L-alpha glycerylphosphorylcholine, α-GPC) increases hippocampal neurogenesis and provides protection against seizure-induced neuronal death and cognitive impairment. *Brain Res.* **2017**, *1654*, 66–76. [CrossRef] [PubMed]
2. Tayebati, S.K. Phospholipid and lipid derivatives as potential neuroprotective compounds. *Molecules* **2018**, *23*, 2257. [CrossRef] [PubMed]

3. Zhang, K.; Wang, X.; Liu, Y. Aqueous medium enzymatic preparation of L-alpha glycerylphosphorylcholine optimized by response surface methodology. *Eur. Food Res. Technol.* **2012**, *234*, 485–491. [CrossRef]
4. Bang, H.; Kim, I.; Kim, B. Phospholipase A(1)-catalyzed hydrolysis of soy phosphatidylcholine to prepare L-alpha-glycerylphosphorylcholine in organic-aqueous media. *Food Chem.* **2016**, *190*, 201–206. [CrossRef] [PubMed]
5. Zhang, K.; Liu, Y.; Wang, X. Enzymatic preparation of L-alpha-glycerylphosphorylcholine in an aqueous medium. *Eur. J. Lipid Sci. Technol.* **2012**, *114*, 1254–1260. [CrossRef]
6. Lim, C.W.; Kim, B.H.; Kim, I.H.; Lee, M.W. Modeling and optimization of phospholipase A(1)-catalyzed hydrolysis of phosphatidylcholine using response surface methodology for lysophosphatidylcholine production. *Biotechnol. Prog.* **2015**, *31*, 35–41. [CrossRef] [PubMed]
7. Kielbowicz, G.; Smuga, D.; Gladkowski, W.; Chojnacka, A.; Wawrzenczyk, C. An LC method for the analysis of phosphatidylcholine hydrolysis products and its application to the monitoring of the acyl migration process. *Talanta* **2012**, *94*, 22–29. [CrossRef] [PubMed]
8. Sheldon, R.A.; van Pelt, S. Enzyme immobilisation in biocatalysis: Why, what and how. *Chem. Soc. Rev.* **2013**, *42*, 6223–6235. [CrossRef] [PubMed]
9. Sheldon, R.A.; Pereira, P.C. Biocatalysis engineering: The big picture. *Chem. Soc. Rev.* **2017**, *46*, 2678–2691. [CrossRef] [PubMed]
10. Bilal, M.; Iqbal, H.M.N.; Guo, S.; Hu, H.; Wang, W.; Zhang, X. State-of-the-art protein engineering approaches using biological macromolecules: A review from immobilization to implementation view point. *Int. J. Biol. Macromol.* **2018**, *108*, 893–901. [CrossRef] [PubMed]
11. Ding, S.; Cargill, A.A.; Medintz, I.L.; Claussen, J.C. Increasing the activity of immobilized enzymes with nanoparticle conjugation. *Curr. Opin. Biotechnol.* **2015**, *34*, 242–250. [CrossRef] [PubMed]
12. Campbell, A.S.; Dong, C.; Meng, F.; Hardinger, J.; Perhinschi, G.; Wu, N.; Dinu, C.Z. Enzyme catalytic efficiency: A function of bio-nano interface reactions. *ACS Appl. Mater. Interfaces* **2014**, *6*, 5393–5403. [CrossRef] [PubMed]
13. Wang, L.; Wang, Y.; He, R.; Zhuang, A.; Wang, X.; Zeng, J.; Hou, J.G. A new nanobiocatalytic system based on allosteric effect with dramatically enhanced enzymatic performance. *J. Am. Chem. Soc.* **2013**, *135*, 1272–1275. [CrossRef] [PubMed]
14. Wu, X.; Ge, J.; Yang, C.; Hou, M.; Liu, Z. Facile synthesis of multiple enzyme-containing metal-organic frameworks in a biomolecule-friendly environment. *Chem. Commun.* **2015**, *51*, 13408–13411. [CrossRef] [PubMed]
15. Lyu, F.; Zhang, Y.; Zare, R.N.; Ge, J.; Liu, Z. One-pot synthesis of protein-embedded metal-organic frameworks with enhanced biological activities. *Nano Lett.* **2014**, *14*, 5761–5765. [CrossRef] [PubMed]
16. He, J.; Sun, S.; Zhou, Z.; Yuan, Q.; Liu, Y.; Liang, H. Thermostable enzyme-immobilized magnetic responsive Ni-based metal-organic framework nanorods as recyclable biocatalysts for efficient biosynthesis of S-adenosylmethionine. *Dalton Trans.* **2019**, *48*, 2077–2085. [CrossRef] [PubMed]
17. Nowroozi-Nejad, Z.; Bahramian, B.; Saman Hosseinkhani, S. Efficient immobilization of firefly luciferase in a metal organic framework: Fe-MIL-88(NH_2) as a mighty support for this purpose. *Enzym. Microb. Technol.* **2019**, *121*, 59–67. [CrossRef] [PubMed]
18. Wang, Y.; Zhang, N.; Zhang, E.; Han, Y.; Qi, Z.; Ansorge-Schumacher, M.B.; Ge, Y.; Wu, C. Heterogeneous metal-organic-framework-based biohybrid catalysts for cascade reactions in organic solvent. *Chem. Eur. J.* **2019**, *25*, 1716–1721. [CrossRef] [PubMed]
19. Liu, X.; Chen, W.; Lian, M.; Chen, X.; Lu, Y.; Yang, W. Enzyme immobilization on ZIF-67/MWCNT composite engenders highsensitivity electrochemical sensing. *J. Electroanal. Chem.* **2019**, *833*, 505–511. [CrossRef]
20. Zare, A.; Bordbar, A.; Razmjou, A.; Jafarian, F. The immobilization of *Candida rugosa* lipase on the modified polyethersulfone with MOF nanoparticles as an excellent performance bioreactor membrane. *J. Biotechnol.* **2019**, *289*, 55–63. [CrossRef] [PubMed]
21. Nadar, S.S.; Rathod, V.K. Magnetic-metal organic framework (magnetic-MOF): A novel platform for enzyme immobilization and nanozyme applications. *Int. J. Biol. Macromol.* **2018**, *120*, 2293–2302. [CrossRef] [PubMed]
22. Ling, P.; Qian, C.; Gao, F.; Lei, J. Enzyme-immobilized metal-organic framework nanosheets as tandem catalysts for the generation of nitric oxide. *Chem. Commun.* **2018**, *54*, 11176–11179. [CrossRef] [PubMed]

23. Cui, J.; Ren, S.; Sun, B.; Jia, S. Optimization protocols and improved strategies for metal-organic frameworks for immobilizing enzymes: Current development and future challenges. *Coord. Chem. Rev.* **2018**, *370*, 22–41. [CrossRef]
24. Lian, X.; Fang, Y.; Joseph, E.; Wang, Q.; Li, J.; Banerjee, S.; Lollar, C.; Wang, X.; Zhou, H.C. Enzyme-MOF (metal-organic framework) composites. *Chem. Soc. Rev.* **2017**, *46*, 3386–3401. [CrossRef] [PubMed]
25. Majewski, M.B.; Howarth, A.J.; Li, P.; Wasielewski, M.R.; Hupp, J.T.; Farha, O.K. Enzyme encapsulation in metal-organic frameworks for applications in catalysis. *CrystEngComm* **2017**, *19*, 4082–4091. [CrossRef]
26. Wu, X.; Yang, C.; Ge, J. Green synthesis of enzyme/metal-organic framework composites with high stability in protein denaturing solvents. *Bioresour. Bioprocess.* **2017**, *4*, 24–24. [CrossRef] [PubMed]
27. Chen, C.; Sun, W.; Lv, H.; Li, H.; Wang, Y.; Wang, P. Spacer arm-facilitated tethering of laccase on magnetic polydopamine nanoparticles for efficient biocatalytic water treatment. *Chem. Eng. J.* **2018**, *350*, 949–959. [CrossRef]
28. Wu, L.; Wu, S.; Xu, Z.; Qiu, Y.; Li, S.; Xu, H. Modified nanoporous titanium dioxide as a novel carrier for enzyme immobilization. *Biosens. Bioelectron.* **2016**, *80*, 59–66. [CrossRef] [PubMed]
29. Pu, S.; Zhang, X.; Yang, C.; Naseer, S.; Zhang, X.; Ouyang, J.; Li, D.; Yang, J. The effects of NaCl on enzyme encapsulation by zeolitic imidazolate frameworks-8. *Enzym. Microb. Technol.* **2019**, *122*, 1–6. [CrossRef] [PubMed]
30. Bilal, M.; Adeel, M.; Rasheed, T.; Iqbal, H.M.N. Multifunctional metal–organic frameworks-based biocatalytic platforms: Recent developments and future prospects. *J. Mater. Res. Technol.* **2018**. [CrossRef]
31. Bilal, M.; Zhao, Y.; Noreen, S.; Shah, S.Z.H.; Bharagava, R.N.; Iqbal, H.M.N. Modifying bio-catalytic properties of enzymes for efficient biocatalysis: A review from immobilization strategies viewpoint. *Biocatal. Biotransform.* **2019**. [CrossRef]
32. Bilal, M.; Rasheed, T.; Zhao, Y.; Iqbal, H.M.N.; Cui, J. "Smart" chemistry and its application in peroxidase immobilization using different support materials. *Int. J. Biol. Macromol.* **2018**, *119*, 278–290. [CrossRef] [PubMed]
33. Bilal, M.; Asgher, M.; Cheng, H.; Yan, Y.; Iqbal, H.M.N. Multi-point enzyme immobilization, surface chemistry, and novel platforms: A paradigm shift in biocatalyst design. *Crit. Rev. Biotechnol.* **2019**, *39*, 202–219. [CrossRef] [PubMed]
34. Cao, X.; Ni, Y.; Zhang, A.; Xu, S.; Chen, K.; Ouyang, P. Encapsulation of enzymes in metal ion-surfactant nanocomposites for catalysis in highly polar solvents. *Chem. Commun.* **2017**, *53*, 3134–3137. [CrossRef] [PubMed]
35. Li, H.; Ni, Y.; Cao, X.; He, X.; Li, G.; Chen, K.; Ouyang, P.; Yang, J.; Tan, W. Highly active nanobiocatalysis in deep eutectic solvents via metal-driven enzyme-surfactant nanocomposite. *J. Biotechnol.* **2019**, *292*, 39–49. [CrossRef] [PubMed]
36. Li, H.; Pang, Y.; Wang, X.; Cao, X.; He, X.; Chen, K.; Li, G.; Ouyang, P.; Tan, W. Phospholipase D encapsulated into metalsurfactant nanocapsules for enhancing biocatalysisin a two-phase system. *RSC Adv.* **2019**, *9*, 6548–6555. [CrossRef]
37. Mashimo, Y.; Mie, M.; Kobatake, E. A DNA-scaffold platform enhances a multi-enzymatic cycling reaction. *Biotechnol. Lett.* **2018**, *40*, 667–672. [CrossRef] [PubMed]
38. Zhu, Y.Y.; Lan, G.; Fan, Y.; Veroneau, S.S.; Song, Y.; Micheroni, D.; Lin, W. Merging photoredox and organometallic catalysts in a metal-organic framework significantly boosts photocatalytic activities. *Angew. Chem. Int. Ed.* **2018**, *57*, 14090–14094. [CrossRef] [PubMed]
39. Denis, J.D.S.; Liew, S.K.; Scully, C.C.G.; Yudin, A.K. Activation of alkynylzinc reagents by a hemiaminal-driven catalytic microenvironment. *Eur. J. Org. Chem.* **2017**, *2*, 419–423. [CrossRef]
40. Chai, Y.; Liu, S.; Zhao, Z.J.; Gong, J.; Dai, W.; Wu, G.; Guan, N.; Li, L. Selectivity modulation of encapsulated palladium nanoparticles by zeolite microenvironment for biomass catalytic upgrading. *ACS Catal.* **2018**, *8*, 8578–8589. [CrossRef]
41. Pavlovic, M.; Rouster, P.; Szilagyi, I. Synthesis and formulation of functional bionanomaterials with superoxide dismutase activity. *Nanoscale* **2017**, *9*, 369–379. [CrossRef] [PubMed]
42. Li, X.; Gao, X.; Ai, L.; Jiang, J. Mechanistic insight into the interaction and adsorption of Cr(VI) with zeolitic imidazolate framework-67 microcrystals from aqueous solution. *Chem. Eng. J.* **2015**, *274*, 238–246. [CrossRef]
43. Wu, X.; Yang, C.; Ge, J.; Liu, Z. Polydopamine tethered enzyme/metal-organic framework composites with high stability and reusability. *Nanoscale* **2015**, *7*, 18883–18886. [CrossRef] [PubMed]

44. Zhou, X.; Gao, Y.; Deng, S.; Cheng, S.; Zhang, S.; Hu, H.; Zhuang, G.; Zhong, X.; Wang, J. Improved oxygen reduction reaction performance of Co confined in ordered N-doped porous carbon derived from ZIF-67@PILs. *Ind. Eng. Chem. Res.* **2017**, *56*, 11100–11110. [CrossRef]
45. Yang, Q.; Ren, S.; Zhao, Q.; Lu, R.; Hang, C.; Chen, Z.; Zheng, H. Selective separation of methyl orange from water using magnetic ZIF-67 composites. *Chem. Eng. J.* **2018**, *333*, 49–57. [CrossRef]
46. Sun, Y.; Yang, Z.; Zhang, L.; Zhou, N.; Weng, S.; Wu, J. The Interaction of Co^{2+} ions and sodium deoxycholate micelles. *J. Mol. Struct.* **2003**, *655*, 321–330. [CrossRef]
47. Zhang, B.; Li, P.; Zhang, H.; Wang, H.; Li, X.; Tian, L.; Ali, N.; Ali, Z.; Zhang, Q. Preparation of lipase/$Zn_3(PO_4)_2$ hybrid nanoflower and its catalytic performance as an immobilized enzyme. *Chem. Eng. J.* **2016**, *291*, 287–297. [CrossRef]
48. Xia, T.T.; Lin, W.; Liu, C.Z.; Guo, C. Improving catalytic activity of laccase immobilized on the branched polymer chains of magnetic nanoparticles under alternating magnetic field. *J. Chem. Technol. Biotechnol.* **2018**, *93*, 88–93. [CrossRef]
49. Madhu, H.C.; Kumar, P.A.; Perugu, C.S.; Kailas, S.V. Microstructure and mechanical properties of friction stir process derived Al-TiO_2 nanocomposite. *J. Mater. Eng. Perform.* **2018**, *27*, 1318–1326. [CrossRef]
50. Cheng, H.P.; Hu, M.C.; Zhai, Q.G.; Li, S.N.; Jiang, Y.C. Polydopamine tethered CPO/HRP-TiO_2 nano-composites with high bio-catalytic activity, stability and reusability: Enzyme-photo bifunctional synergistic catalysis in water treatment. *Chem. Eng. J.* **2018**, *347*, 703–710. [CrossRef]
51. Cohen, J.L.; Karav, S.; Barile, D.; Bell, J.M.L.N.D. Immobilization of an endo-beta-N-acetylglucosaminidase for the release of bioactive N-glycans. *Catalysts* **2018**, *8*, 278. [CrossRef]